

Formation and break-up of rigid agglomerates in turbulent channel and pipe flows

Schutte, K. C.J.; Portela, L. M.; Twerda, A.; Henkes, R. A.W.M.

DOI

[10.1017/jfm.2018.716](https://doi.org/10.1017/jfm.2018.716)

Publication date

2018

Document Version

Accepted author manuscript

Published in

Journal of Fluid Mechanics

Citation (APA)

Schutte, K. C. J., Portela, L. M., Twerda, A., & Henkes, R. A. W. M. (2018). Formation and break-up of rigid agglomerates in turbulent channel and pipe flows. *Journal of Fluid Mechanics*, *857*, 539-561. <https://doi.org/10.1017/jfm.2018.716>

Important note

To cite this publication, please use the final published version (if applicable). Please check the document version above.

Copyright

Other than for strictly personal use, it is not permitted to download, forward or distribute the text or part of it, without the consent of the author(s) and/or copyright holder(s), unless the work is under an open content license such as Creative Commons.

Takedown policy

Please contact us and provide details if you believe this document breaches copyrights. We will remove access to the work immediately and investigate your claim.

Formation and break-up of rigid agglomerates in turbulent channel and pipe flows

K. C. J. Schutte¹, L. M. Portela¹, A. Twerda^{2,3} and R. A. W. M. Henkes^{2†}

¹Department of Chemical Engineering, Delft University of Technology, Post Office Box 5, 2600 AA Delft, The Netherlands

²Process & Energy Department, Delft University of Technology, Post Office Box 5, 2600 AA Delft, The Netherlands

³TNO, Post Office Box 6012, 2600 JA Delft, Netherlands

(Received 5 May 2017; revised 24 June 2018; accepted 1 September 2018)

We have developed and applied an Eulerian-Lagrangian model for the transport, formation, break-up, deposition and re-entrainment of particle agglomerates. In this paper, we focus on agglomeration and break-up. Simulations were carried out to investigate what changes in the turbulent flow are inflicted by the presence of the agglomerates. Also, the dependence of the properties of the agglomerates on the Reynolds number of the flow and on the strength of the bonds between the primary particles is studied. The presence of the agglomerates attenuates the turbulence and thereby lowers the Reynolds stresses. As a result, the flow rate increases at constant pressure drop when agglomerates are formed (up to a certain dimension). If the agglomerates surpass this dimension, long-distance viscosity effects become dominant and a flow rate decrease occurs. The characteristics of the agglomerates are largely insensitive to the Reynolds number, provided the flow is turbulent. The agglomerates have an open and porous structure, and a fractal dimension of 1.8–2.3. Their mean mass scales exponentially with the strength of the internal bonds. Contrary to assumptions that are typically made in engineering models in the literature, agglomerates do not preferentially break into two fragments of similar size.

Key words: Multiphase and Particle-laden Flows

1. Introduction

The formation, break-up, deposition and re-entrainment of agglomerates are of major interest in several fields of science and industry. Medical relevancy, such as the formation of thrombosis or atherosclerosis, pollution transport in the atmosphere and flow assurance in the oil and gas industry are only a few examples of where these processes play a role. To predict if, where and/or when these phenomena will occur, simulations using numerical models are a versatile and cost-effective modality. To keep the effort that is required to conduct such simulations tractable, however, simplifications need to be made, either in the scope of the problem statement, or in the representation of the microscopic phenomena. It is our aim to bridge the gap between simulations with a

† Email address for correspondence: r.a.w.m.henkes@tudelft.nl

detailed description of agglomeration and break-up (that are present in the literature as will be described shortly) and turbulent flows.

Meakin & Jullien (1988) numerically studied the formation of agglomerates for three different regimes, fully resolving the structure of the agglomerates in time. These regimes are: random-walk induced collisions between particles and/or agglomerates, with a collision efficiency of unity (Diffusion Limited Agglomeration); collisions induced by linear motion, also with uniform collision efficiency (Ballistic Agglomeration); and rotating two agglomerates over random angles, bringing a pre-defined pair of primary particles into contact, and rejecting the agglomeration event if other primary particles of the agglomerates overlap (Reaction Limited Agglomeration). The different regimes lead to agglomerates with fractal dimensions of approximately 1.80, 1.95 and 2.10, respectively. Meakin & Jullien (1988) also studied how the fractal dimension of the agglomerates changes when restructuring of the agglomerates is allowed for a short period after the initial contact is formed. Maximum fractal dimensions of 2.18, 2.19 and 2.25 were found under those conditions, respectively.

Richardson (1995) studied the formation of agglomerates from an initial state of randomly dispersed primary particles with a random velocity distribution. Different levels of detail were taken into account by Richardson, with the simplest representing all agglomerates by spheres with different masses but identical radii and the most detailed representing the full structure of the agglomerates. Large variations in the agglomeration dynamics between these levels of detail were found, leading to the conclusion that aggregates grow and collide much more effectively than single particles, owing to their complex shape. Mäkinen (2005) constructed a model similar to that of Richardson and also determined the stress in the bonds between the individual primary particles.

Chen & Doi (1999) studied the dissociation of aggregating colloids in strongly-sheared flows, at low Reynolds numbers. Ernst *et al.* (2013) used Lattice-Boltzmann simulations to fully resolve the flow primary particles that are settling in a quiescent fluid. Due to the very fine grid resolution required, only a very limited number of primary particles can be used in such simulations; therefore, Ernst *et al.* used only 50 particles. Zinchenko & Davis (2014) studied a similar system, using a multi-pole solution technique for the Stokes flow around the agglomerates, with agglomerates that consist of up to 100 primary particles. Derksen (2008) studied the forces induced in the bond inside a sphere doublet that is immersed in a turbulent flow, but did not study the dynamics of the formation and/or break-up of the agglomerate.

In the literature that deals with the formation and/or break-up of agglomerates in turbulent flows (e.g. Brunk *et al.* (1998), Flesch *et al.* (1999), Reade & Collins (2000), Babler (2008), de Bona *et al.* (2014), Babler *et al.* (2015)), it is commonplace to neglect the internal agglomerate structure, for instance by using population balance equations. Exception to this are the works of Derksen (2012) and Dizaji & Marshall (2016). Derksen (2012) used an immersed boundary method to model the interaction between homogeneous isotropic turbulence and the process of agglomeration in detail. In that work, a square-well potential is used to model the particle-particle interactions and a maximum of 5000 primary particles is considered, that form agglomerates that consist of up to 150 primary particles. Dizaji & Marshall (2016) studied the formation and break-up of agglomerates in homogeneous turbulence using a discrete element method, with little under 47 000 particles in a cubic box. Agglomerates that consist $\mathcal{O}(200)$ primary particles are formed, with a fractal dimension of 2.3. Both Derksen (2012) and Dizaji & Marshall (2016) did not study how the presence of the agglomerates affect the turbulence, however.

Bridging the gap between a detailed description of agglomeration and break-up and

turbulent flows allows us to assess whether the universality of agglomerate properties that are formed under no-flow or non-turbulent flow conditions still hold if the flow is turbulent. It will also reveal what changes the presence of a dispersed phase that undergoes agglomeration and break-up impose upon the turbulent flow itself. Two typical flow geometries used in numerical turbulence studies (namely an infinite channel and a cylindrical pipe) will be considered to study whether the shape of the flow domain has any influence on the results. We focus our study on agglomerates that have a very small relative inertia compared to the fluid phase.

2. Theory and Methods

2.1. Model basis

The basis of our model is given by an existing particle-laden finite-volume code, called Direct Eulerian-Lagrangian Flow Turbulence (DELFT) (Portela & Oliemans 2003). This code was built as an extension of single-phase finite-volume codes for pipe and channel flows (Eggels 1994; Pourquié 1994; Boersma 1997; van Haarlem 2000) and it can be used both for DNS and LES. In the LES mode, the Smagorinsky model, together with van Driest damping of the eddy viscosity near the walls, is applied to account for the sub-grid turbulence scales.

From a computational perspective, resolving the flow around the individual agglomerates is not a viable option. Instead, the dispersed-phase is solved using a point-particle method based on the particle-source in cell approach (Chen *et al.* 1998), which allows for simulations with one-way and two-way coupling. For efficient detection of particle collisions it uses a methodology similar to the one used by Li *et al.* (2001), described in detail by Chen *et al.* (1998). The DELFT code was used in numerous studies (e.g. Portela *et al.* (2002)) and the point-particle method, with small variations among different authors, is now a standard approach (Marchioli *et al.* 2008).

2.2. Model for particle-particle collisions

Physically, the probability of particles adhering during a collision event depends on the relative time scales involved with the adhesion process and with the particle contact. Since these time scales are much smaller than the largest time scale present in the turbulent flow (which determines the time that needs to be simulated to get a decent statistical accuracy), it is computationally not feasible to model the inter-particle collisions in microscopic detail. Instead, a collision efficiency equal to unity is assumed (the “hit-and-stick” approach). As we only consider agglomeration in competition with break-up, the simplification from a pragmatic perspective is a fair approximation, as, at least to some extent, physically improper agglomeration events will quickly be undone by the break-up of the bonds formed.

All collisions are considered to be purely inelastic, conserving both linear and angular momentum. From time-step to time-step, the agglomerate motion is described by a superposition of the linear velocity of the centre of mass of the agglomerate and the rotation of the agglomerate around its centre of mass. Within time-steps, a second-order accurate approximation of the primary particle trajectory is used to determine which primary particles collide at what moment. These collisions are processed consecutively as they occur, irrespective of the time-step used for agglomerates that momentarily do not undergo collisions. The inter-particle bonds are considered to have an infinite resistance to deformation, resulting in agglomerates that are rigid up to the point where the bonds

between individual particles are broken. Further details about the method can be found in Schutte (2016).

2.3. Hydrodynamic forces acting on dispersed phase

The motion of a particle, that is dispersed inside an unsteady flow at small Reynolds numbers, is well described by the Basset-Boussinesq-Oseen equation, which, neglecting the Faxen force (viz. flow non-uniformity), is given by (Crowe *et al.* 1997):

$$\rho_p \frac{4\pi R_p^3}{3} \frac{d\mathbf{U}_p}{dt} = \underbrace{6\pi\mu_f R_p (\mathbf{U}_f - \mathbf{U}_p)}_{\text{drag}} + \underbrace{\frac{\rho_f}{2} \frac{4\pi R_p^3}{3} \left(\frac{D\mathbf{U}_f}{Dt} - \frac{d\mathbf{U}_p}{dt} \right)}_{\text{added mass}} - \underbrace{\frac{4\pi R_p^3}{3} (\nabla P - \nabla \cdot \mathbf{T})}_{\text{pressure gradient}} + \underbrace{6\sqrt{\pi\rho_f\mu_f} R_p^2 \int_{t_0}^t \frac{1}{\sqrt{t-\tau}} \left[\frac{d\mathbf{U}_f}{d\tau} - \frac{d\mathbf{U}_p}{d\tau} \right] d\tau}_{\text{history force}} + \mathbf{F}_{\text{other}} \quad (2.1)$$

where R_p is the primary particle radius, μ_f the fluid viscosity and ρ_p and ρ_f denote the density of the dispersed and fluid phases, respectively. P presents the pressure and \mathbf{T} is the stress tensor in the fluid. The fluid-phase velocity \mathbf{U}_f is evaluated at the location of the particle centre. The other forces, represented by $\mathbf{F}_{\text{other}}$, may include external forces, such as the gravitational force or an electromagnetic force, or other fluid forces, such as the lift force.

We are particularly interested in simulating upward vertical flows of systems that have density ratios between the dispersed and continuous phases close to one. As a result, gravity does not have a component in the wall-normal direction, and the streamwise gravity-induced slip velocity of the particles is negligible when compared to typical turbulent velocity fluctuations. Likewise, it is expected that the influence of the lift force is small, such that this force can also be neglected. The only force acting on the dispersed phase considered in this work is the drag force, corrected for the added mass effect.

The drag force is approximated using Stokes drag, without accounting for shielding effects for primary particles that are close to each other (the 'free-draining' approximation). Due to the high local particle-concentration inside the agglomerates, shielding effects in reality will have an substantial impact on the force exerted on the primary particles. This effect, however, is complex to model, and computationally very costly to evaluate. Taking it into account would prevent simulating large ensembles of primary particles in turbulent flows within tractable simulation time, as is shown by the state of the art in the literature. Therefore, these detailed local particle-fluid interactions have not been taken into account in our model.

In general, one may expect that the drag force on a particle that is directly exposed to the flow is slightly enhanced due to the presence of a sheltered particle downstream of it, whereas the drag force on the sheltered particle itself can significantly decrease. The overestimation of the total drag force introduced by neglecting these effects is partly compensated by the fact that we use Stokes drag to compute the drag force on individual primary particles. For typical values of the particle Reynolds numbers in our work (up to 10), the Stokes drag approximation under-estimates the drag force on a single sphere.

As a final simplification, we neglect the material derivative of the fluid velocity in the added mass term. This simplification is made for reasons of computational efficiency, as it greatly reduces the number of fluid velocity interpolations that need to be made for

all primary particles during each time-step. Equation (2.1) then reduces to:

$$\check{\rho}_p \frac{4\pi R_p^3}{3} \frac{d\mathbf{U}_p}{dt} \equiv \mathbf{F}_p = 6\pi\mu_f R_p (\mathbf{U}_f - \mathbf{U}_p) \quad \text{with} \quad \check{\rho}_p = \left(\rho_p + \frac{\rho_f}{2} \right) \quad (2.2)$$

where $\check{\rho}_p$ can be seen as the effective density of the dispersed phase corrected for the added mass effect. We have verified that the properties of the steady-state agglomerate population formed does not change significantly when the lift force and the full formulation of the added mass are included in the model, showing that the simplifications made above are reasonable. Order of magnitude estimates that support this result are available online in the supplemental material.

2.4. Break-up

Macroscopically, five principal modes of stress which can give rise to the structural failure of a rigid body can be distinguished: *buckling*, *straining*, *shearing*, *bending* and *twisting*. Buckling and straining are associated with the normal component of the force exerted on the body, and shearing with the tangential force component. Bending and twisting are associated with the normal and tangential components of the exerted torque, respectively. On a microscopic level, shearing, bending, twisting and buckling may lead to internal restructuring of the material (which cannot be taken into account by our model), but by itself, this will not lead to macroscopic failure of the body. Therefore, we consider inter-particle bonds to be broken only when they are at least infinitesimally strained. This ensures that the resulting fragments move apart after the break-up event.

The internal stresses in the bonds between the primary particles are computed by equating the mass times the acceleration of the individual primary particles to the force balance over the respective particles themselves. This technique was also used by Mäkinen (2005):

$$m_p \frac{d\mathbf{U}_p}{dt} = m_p \left(\frac{d\mathbf{U}_{cm}}{dt} + \frac{d\boldsymbol{\Omega}}{dt} \times \mathbf{r}_p + \boldsymbol{\Omega} \times \frac{d\mathbf{r}_p}{dt} \right) = \mathbf{F}_p + \sum_b \mathbf{F}_b \quad (2.3)$$

where the subscript *cm* denotes the centre of mass and $\boldsymbol{\Omega}$ the angular velocity of the agglomerate. The summation in equation (2.3) runs over all bonds the particle *p* has with other primary particles ('nearest-neighbours'), and the values of \mathbf{F}_b represents the force induced in those bonds. Similarly, the torque \mathbf{T}_b in each bond can be found using the equation:

$$\mathbf{I}_p \frac{d\boldsymbol{\Omega}}{dt} - \boldsymbol{\Omega} \times (\mathbf{I}_p \boldsymbol{\Omega}) = \mathbf{F}_p \times \mathbf{r}_p + \sum_b \mathbf{T}_b \quad (2.4)$$

which is defined in a co-rotating reference frame attached to the individual agglomerates. \mathbf{I}_p represents the moment of inertia tensor of the particle about the centre of mass of the agglomerate and \mathbf{r}_p is the location vector of the primary particle with respect to the agglomerate centre of mass.

Evaluating expressions (2.3) and (2.4) for all primary particles in an agglomerate results in two systems of N equations. Since we consider agglomerates to be rigid, and fully resolve collisions in time, the probability that two agglomerates connect at more than one pair primary particle is infinitesimally small (Gastaldi & Vanni 2011). Primary particles thus are connected by one unique pathway only, and in an agglomerate that consists of N particles, exactly $N - 1$ bonds are present. Hence, the systems of equations are always closed. Bonds are considered to be broken when any of the normal or tangential stress components exceed threshold values that are characteristic for the strength of the bonds (viz. $(\mathbf{F}_b)_\perp > F_L^N$ for straining, $(\mathbf{F}_b)_\parallel > F_L^S$ for shearing, $(\mathbf{T}_b)_\perp > T_L^B$ for

bending or $(\mathbf{F}_b)_\parallel > T_L^T$ for twisting), provided that the fragments move apart afterwards. If multiple bonds in one agglomerate are eligible for break-up at the same time, the bond to be actually broken is selected randomly. The linear and angular velocities of the agglomerate branches after break-up are set such that the velocity of the primary particles does not change instantaneously during the breakage. This corresponds to conservation of linear and angular momentum.

It is important to emphasize that the adhesion mechanisms that are considered in this work are more complex than for instance considered in the JKR theory (Johnson *et al.* 1971). Such complex adhesion may occur, for example, whenever partial recrystallization plays a role in the formation of bonds between the primary particles. This is also the reason that shearing, bending and twisting may lead to the break-up of an agglomerate; these are not covered by simple contact models, where only straining can lead to agglomerate fragmentation.

2.5. Interaction between particles and wall

Collisions between agglomerates and the walls of the flow domain are resolved in time. In each collision, the linear and angular velocities of the agglomerates are changed such that the wall-normal velocity component (W_p) of the primary particle that has collided with the wall is reversed. In the limit of an agglomerate that consists only of one primary particle, this corresponds to a specular reflection. To ensure that particles that have virtually no wall-normal velocity and a relatively large wall-normal acceleration do not 'float' into the wall during the remainder of the numerical time-step (Δt_{rest}), the target for the wall-normal velocity of the particle after the collision is computed as:

$$W_{\text{target}} = \begin{cases} -\frac{1}{2}(1 + \epsilon) \frac{dW_p^o}{dt} & \text{if } |W_p^o| < \frac{1}{2}(1 + \epsilon) \left| \frac{dW_p^o}{dt} \right| \Delta t_{\text{rest}} \\ -W_p^o & \text{if } |W_p^o| > \frac{1}{2}(1 + \epsilon) \left| \frac{dW_p^o}{dt} \right| \Delta t_{\text{rest}} \end{cases} \quad (2.5)$$

where $\epsilon = 10^{-6}$. This is a simple fix to ensure that particles remain inside the computational domain (lying almost exactly flush with the wall after Δt_{rest}), removing the need to take very small time steps for those particles that are really close to the wall. If the agglomerate consists of more than one primary particle, the specular reflection results both in a linear and angular impulse acting on the agglomerate. The expressions for both of these are given in Schutte (2016).

2.6. Two-way coupling between fluid and dispersed phases

Like Portela & Oliemans (2003), who used the DELFT code with two-way coupling for spherical particles, we model the force exerted by the dispersed phase on the continuous (fluid) phase by using Newton's third law. For agglomerates that extend over multiple fluid-phase grid-cells, the backforcing in each of the control volumes is computed by summing only the contributions of the primary particles that have their centre located inside that control volume. Thereby, the backforcing of the agglomerate is spread out over the grid-cells that the agglomerate spans, and no excessive backforcing occurs in individual control volumes.

3. Description of considered cases

3.1. Flow properties

We consider turbulent channel and pipe flows with $Re_\nabla (\equiv \rho_f u_\nabla H / \mu_f)$ equal to 360 and 720, corresponding to bulk Reynolds numbers between 5400 and 12 500. The pressure

TABLE 1. Overview of parameters associated with the continuous phase flow.

	Channel		Pipe	
Re_{∇}	360	720	360	720
Re_{bulk} (unladen/one-way coupling)	5700	12 500	5400	12 400
$(n_x, n_{\theta}, n_r) = (192, 128, 64)$			DNS	LES
$(n_x, n_y, n_z) = (192, 128, 96)$	DNS	LES (two-way)		
$(n_x, n_y, n_z) = (320, 224, 160)$		DNS (one-way)		
$L_x, L_y/\theta, H/R$	5, 2, 1		5, 2π , 0.5	

TABLE 2. Grid resolutions considered in this work, expressed in wall units. Values printed in regular typeface represent grids that are used for DNS, and values in italics represent grids that are used for LES. The sequences of values reported correspond to $Re_{\nabla} = 360$ and $Re_{\nabla} = 720$.

Grid $(n_x, n_{y/\theta}, n_z/R)$	(192, 128, 64)	(192, 128, 96)	(320, 224, 160)
Δ_x^+	9.4, <i>18.8</i>	9.4, <i>18.8</i>	-, 11
Δ_y^+	not applicable	5.6, <i>11.3</i>	-, 6.4
$\Delta_{z/r}^+ _{\text{wall}}$	1.1, <i>2.2</i>	1.2, <i>2.3</i>	-, 1.2
$\Delta_{z/r}^+ _{\text{centre}}$	4.3, <i>9.5</i>	4.8, <i>9.7</i>	-, 5.8

gradient velocity u_{∇} is defined as:

$$u_{\nabla} = \sqrt{-\frac{1}{G} \frac{\partial \bar{P}}{\partial x} \frac{H}{\rho_f}} \quad (3.1)$$

where G is equal to 2 in the channel and 4 in the pipe; H represents the pipe radius or the full channel height and $\partial \bar{P}/\partial x$ is the pressure gradient that is the driving force of the flow. Periodic boundary conditions are used in the streamwise (x) and spanwise/circumferential (y/θ) directions. For the fluid flow, a no-slip boundary condition is used at the walls, that are located at $z = 0.0$ and $z = 1.0$ in the channel and at $r = 0.5$ in the pipe. A uniform grid is used in the streamwise and spanwise/circumferential directions. In the wall-normal direction, the resolution is higher near the walls than in the centre, transitioning gradually. Care is taken to ensure that the turbulent flow is statistically steady before the dispersed phase is introduced.

The parameters associated with the fluid phase are summarized in table 1. The associated grid resolutions (in wall units), are given in table 2. The grid resolutions used in the channel are similar or better than the ones used by van Haarleem (2000) in DNS studies with the DELFT code. The grid resolutions used in DNS mode in the pipe are similar to the ones used by Eggels (1994).

3.2. Dispersed-phase parameters

The dispersed-phase parameters are given by: the radius of the primary particles (R_p), the volume fraction and number of primary particles, the added-mass corrected particle-fluid density ratio ($\check{\rho}_p/\rho_f$), and the maximum stress that the inter-particle bonds can withstand before breaking (F_L^N , F_L^S , T_L^B and T_L^T), as explained in Section 2.4.

In this study, we consider particles that are mono-disperse, with a radius equal to 0.5% of the channel height H . This relatively large primary particle size is adopted because it results in sufficiently large collision rates at moderate primary particle numbers, allowing the simulations to reach a steady-state within a reasonable simulation time. In each channel flow simulation, we introduce 250 000 primary particles, corresponding to a dispersed phase volume fraction of 1.3%. In pipe flows, the same dispersed phase volume fraction is used by lowering the number of primary particles to 98 175. The particles are individually introduced at random locations throughout the entire flow domain; their initial velocity is set equal to the local fluid velocity. The density ratio ρ_p/ρ_f is set at 1.5. This gives an effective, added-mass corrected density ratio $\check{\rho}_p/\rho_f$ of 2.0. The dimensions of the computational domain are equal for the dispersed phase and the continuous phase, and periodic boundary conditions are used for the particles in the streamwise and spanwise directions, like they are also used for the continuous phase.

The maximum stress that the inter-particle bonds can withstand before breaking and Re_∇ are the parameters that are varied between simulations. For interpreting the results, we consider the values of F_L and T_L scaled by the characteristic hydrodynamic force acting on a single primary particle in a turbulent flow, which can be obtained by substituting u_∇ for $(\mathbf{U}_f - \mathbf{U}_p)$ in equation (2.2). These can be expressed as:

$$F_L^* = \frac{F_L}{6\pi\mu_f R_p u_\nabla}; \quad T_L^* = \frac{T_L}{6\pi\mu_f R_p^2 u_\nabla} \quad (3.2)$$

Multiple values of F_L^* and T_L^* are considered; their values are chosen such that the number of primary particles per agglomerate in steady-state is of $\mathcal{O}(100)$. This allows, on the one hand, that a significant number of agglomerates can be simulated with a tractable number of primary particles, yet, on the other hand, that it remains feasible to attribute macroscopic properties (e.g. a fractal dimension) to the agglomerates.

Agglomerates are considered to be broken by only one single break-up mechanism in each simulation. This is equivalent to assuming that the bonds between the particles can withstand infinite stresses in all but one stress component (e.g. when agglomerates are broken due to shearing, they are assumed to have an infinite resistance to straining, bending and twisting). Although it is clearly not possible to engineer a physical bond with these properties, this approach allows to study the interaction of the individual stress components with the turbulent flow.

3.3. Simulation conditions

The balance between agglomeration and break-up leads to a statistical steady-state (stationary state); we will simply refer to it as 'steady-state'. When the steady-state sets in, individual agglomerates still frequently undergo collisions, thereby forming larger agglomerates, and agglomerates also are frequently broken. Overall, these processes cancel out each other, such that the properties of the agglomerate population in a statistical sense remain unchanged. The results that are presented in the remainder of this paper refer to average values of steady-state situations, unless otherwise noted.

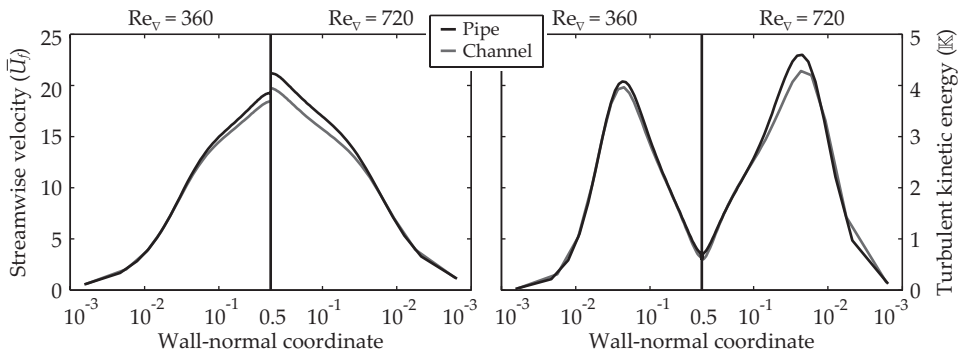


FIGURE 1. Comparison of the non-dimensional time-averaged streamwise velocity (left) and the turbulent kinetic energy (right) for non-laden flows.

4. Non-laden turbulent flow properties

Figure 1 shows a comparison of the time-averaged streamwise fluid velocity and the turbulent kinetic energy as a function of the wall-normal coordinate between non-laden channel and pipe flows. The mean velocity and the turbulent kinetic energy have been normalised with u_{∇} and u_{∇}^2 , respectively.

For the channel, we compared the statistics of the single-phase $Re_{\nabla} = 360$ flow to the DNS reference data by Moser *et al.* (1999). The maximum deviation of the mean streamwise fluid velocity (+1.4%) occurs close to the walls of the channel. The maximum observed deviation in the Reynolds stresses is found for $\overline{u'u'}$ (-12%), close the centre of the channel. For pipe, we compared the statistics of the single-phase $Re_{\nabla} = 360$ flow to the high-resolution DNS data obtained by Khoury *et al.* (2013). We found that the maximum deviation of the mean streamwise fluid velocity (+1.0%) occurs at around $r = 0.2$. The maximum deviation observed in the Reynolds stresses is found for $\overline{w'w'}$ (-8.4%), close the wall of the pipe.

5. Results: Modification of turbulence

When two-way coupling is considered, the presence of the agglomerates will change the properties of the turbulent flow. It is well known from the literature that the addition of non-interacting spherical particles to a turbulent flow may augment (for relatively large particles) or attenuate the turbulence intensity (for smaller particles) (Balachandar & Eaton 2010). The addition of a dispersed phase with non-spherical structures (such as polymers (Sureshkumar *et al.* 1997; Ptasiński *et al.* 2001), or non-elastic rods (Paschke *et al.* 2004)) can cause a drag reduction in turbulent flows by reduction of the turbulent stresses. On the other hand, one may expect that the presence of dispersed objects with dimensions that are large compared to the typical length-scale of the turbulent eddies increase the correlation length of the flow, and thus increase the apparent viscosity of the fluid (which essentially is a measure of the resistance of the fluid against velocity gradients).

5.1. Change of mean flow rate

Figure 2 shows the change in overall flow rate upon lading the flow with the dispersed phase using two-way coupling. To separate between the effects of the general lading and the specific interactions of the agglomerates with the flow, additional results are shown for flows that are laden with two-way coupled non-interacting spherical particles. Apart

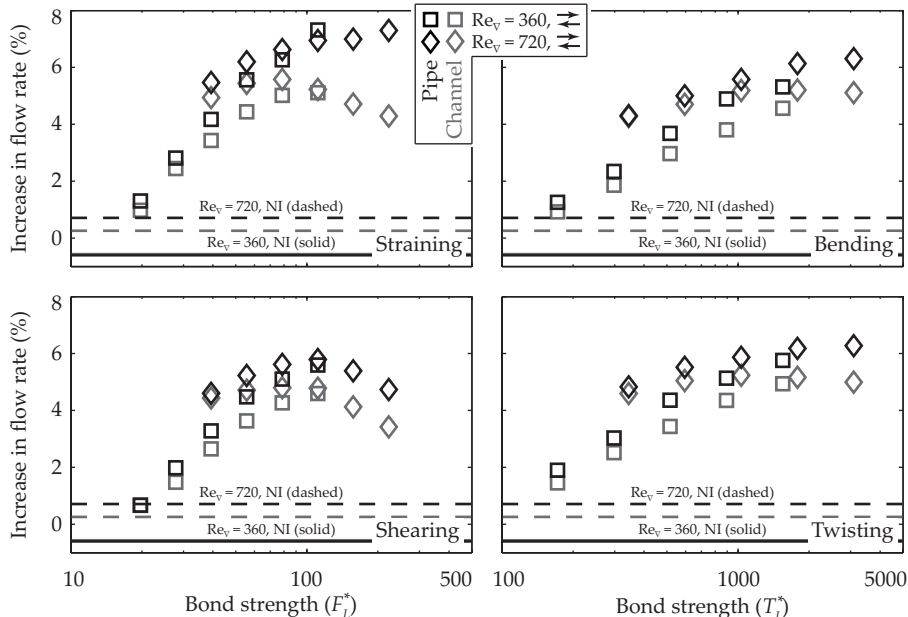


FIGURE 2. Change in fluid-phase flow rate with respect to non-laden flow upon including the dispersed phase using two-way coupling. The horizontal lines indicate results that have been obtained using a two-way coupled non-interacting dispersed phase with the same properties and volume fraction as in the agglomeration/break-up model, for reference.

from being non-interacting, these dispersed phases have the same properties and volume fraction as considered in all other cases.

It is clear that the effect of the agglomerates on the flow by far surpasses the effect of the non-interacting primary particles. The most important observations that can be made are: (I) the maximum increase in the flow rate achieved in the channel (about 5.5%) is smaller than that in the pipe (about 7%); (II) the maximum increase is similar for both Reynolds numbers, yet reached at lower values for F_L^* and T_L^* at $Re_{\nabla} = 720$ than at $Re_{\nabla} = 360$; (III) agglomerates broken by straining inflict the largest influence on the flow, the effect of both torque-related break-up mechanisms is smaller and similar whereas shearing leads to the smallest increases in flow rate.

The increase in flow rate mainly results from an increase in the streamwise velocity near the centre of the channel and the pipe, as is shown in figure 3. If the agglomerate strength surpasses a certain threshold (which is lower in the pipe than in the channel), the largest velocity increase no longer occurs near the centre of the flow domain, but at a location intermediate between the wall and the centre. We postulate that this is caused by the way that the agglomerates affect the effective viscosity of the continuous phase, as will be explained shortly. Note that the stronger increase of fluid velocity close to the walls of the flow domain at $Re_{\nabla} = 720$ compared to $Re_{\nabla} = 360$ may be caused by the by the fact that LES is used at the former Reynolds number. Possibly, its resolution is insufficient to fully capture the changes in the boundary layer induced by the two-way coupling of the dispersed phase.

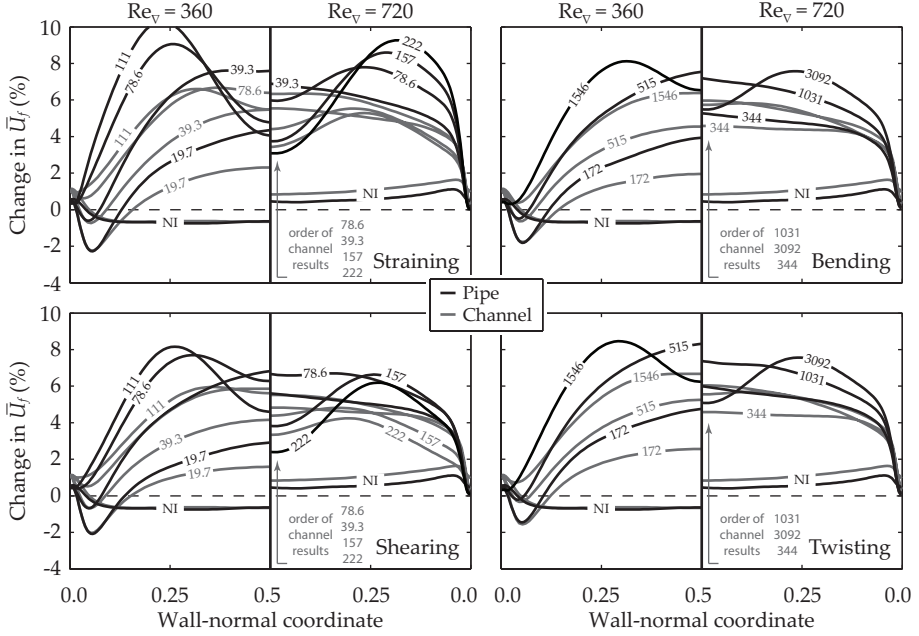


FIGURE 3. Change in the average continuous phase streamwise velocity with respect to non-laden flow upon including dispersed-phase using two-way coupling. The numbers imposed onto the lines indicate the values of F_L^* and T_L^* used to obtain the respective results. ‘NI’ indicates results obtained using a two-way coupled non-interacting dispersed phase.

5.2. Turbulence modification by dispersed phase

As we consider pressure-driven flows and constant molecular viscosities in our simulations, any changes in the effective viscosity of the fluid phase will result in changes in the fluid flow rate. As a simple estimate of how the magnitude of the turbulent viscosity of the continuous phase changes upon two-way coupling with the dispersed phase, we consider the turbulent kinetic energy. Figure 4 shows the change in turbulent kinetic energy as a function of the wall-normal coordinate for the two-way coupled approach compared to non-laden flows. The presence of the dispersed phase that is undergoing agglomeration and break-up has a strong tendency to decrease the turbulent kinetic energy. This tendency is stronger in the pipe than it is in the channel.

At large values of F_L^* and T_L^* , the decrease of the turbulent kinetic energy saturates. As will be shown in section 6.3, the number of primary particles per agglomerate will continue growing upon further increasing the value of F_L^* or T_L^* past this saturation point. Consequently, the dimensions of the agglomerates keep on increasing. As postulated before, a growth of the agglomerates will lead to an increase in the effective fluid viscosity by increasing the correlation length of the flow[†]. This hypothesis is supported by the results of some simulations that were conducted in laminar flows (in which the turbulent eddy viscosity does not play a role), where we find that the flow rate decreases significantly (by around 25%) upon lading the flow with the two-way coupled dispersed phase that is undergoing agglomeration and break-up.

When the turbulent eddy viscosity has already vanished considerable, its further decrease for increasing values of F_L^* and T_L^* can no longer compensate for the increase

[†] Such an increase is indeed observed in our simulations. It is non-isotropic and its magnitude varies as a function of the wall-normal coordinate

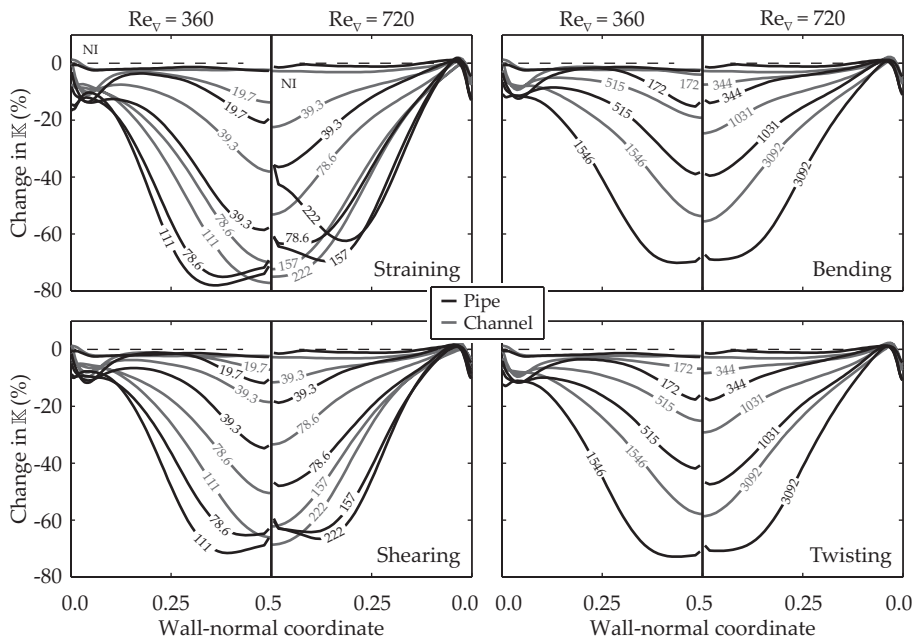


FIGURE 4. Change in the turbulent kinetic energy with respect to non-laden flow, upon including the dispersed phase using two-way coupling. The labels aligned along the lines indicate the values of F_L^* and T_L^* used to obtain the respective results. Black lines: pipe flow, grey lines: channel flow.

of the long-range correlation viscosity. This point marks the transition above which the fluid flow rate decreases upon a further increase of F_L^* or T_L^* . The agglomerates are more effective at suppressing the turbulence fluctuations in the pipe than in the channel at lower values of F_L^* and T_L^* (and thus, as will be shown in section 6.3, when they contain fewer primary particles and have smaller dimensions). Therefore, the balance between both competing effects sets in at larger values of the flow rate increase in the pipe than in the channel. This explains the differences in the maximum flow rate increase in both geometries.

6. Results: Agglomerate properties

In this section, the properties of the agglomerates will be discussed. Since, due to the nature of the model that was adopted, the break-up of agglomerates is intensely linked to the particle-fluid interactions, some of the properties that will be studied are probed during break-up events.

6.1. Slip velocity of primary particles with respect to the continuous phase

Figure 5 shows the magnitude of the average slip velocity of the primary particles, probed at the moment individual agglomerates are broken. The results in figure 5 show that: (I) in general, the slip velocities are larger in the pipe than in the channel; (II) the slip velocities decrease significantly when two-way coupling is considered instead of one-way coupling; (III) under two-way coupling the slip velocities are dependent on the value of Re_{∇} ; and (IV) slip velocities are similar for the different break-up mechanisms.

Since the dispersed phase has a very small non-dimensional density, the agglomerates

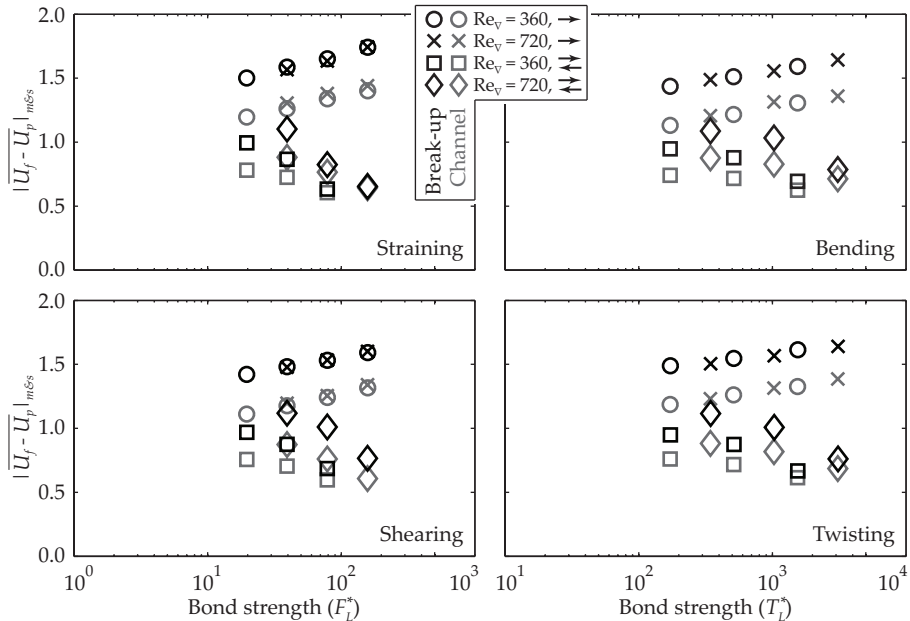


FIGURE 5. Average magnitude of the primary particle slip velocity measured at agglomerate break-up. The quoted values are averages over all primary particles per simulation (not weighted per agglomerate).

adapt quickly to local changes in the fluid flow velocity. Therefore, they act as a spatial filter to the fluid velocity along their perimeter. The more the different branches of one agglomerate protrude through different turbulent eddies, the more the characteristic slip velocity of the primary particles will approach the characteristic velocity difference between these eddies. Due to the curvature of the flow domain, the turbulent inner layer (which is characterised by a large wall-normal streamwise velocity gradient and strong turbulent velocity fluctuations) occupies a larger volumetric fraction of the flow domain in the pipe than it does in the channel. Therefore, it has more opportunity to interact with the dispersed phase. Together, this explains why the average magnitude of the slip velocity of the primary particles is larger in former geometry.

Two-way coupling induces feedback of the velocity filtering experienced by the agglomerates onto the flow. As shown before, this attenuates local fluid velocity fluctuations, which in turn results in a decrease of the average primary-particle slip velocity compared one-way coupling. The stronger attenuation of turbulence by agglomerates with larger values of F_L^* and T_L^* found in section 5.2 is consistent with the growing deviation between the one- and two-way coupled average slip velocities as the strength of the agglomerates is increased.

6.2. Derivation of a simple model for the induced internal stresses in an agglomerate

Rewriting equation (2.3), it follows that the linear stress induced in an arbitrary bond b inside an agglomerate can be written in the form:

$$\begin{aligned} \mathbf{F}_b &= \sum_m \left[\mathbf{F}_p - m_p \left(\frac{d\mathbf{U}_{cm}}{dt} + \frac{d\boldsymbol{\Omega}}{dt} \times \mathbf{r}_p + \boldsymbol{\Omega} \times \frac{d\mathbf{r}_p}{dt} \right) \right] \\ &= - \sum_s \left[\mathbf{F}_p - m_p \left(\frac{d\mathbf{U}_{cm}}{dt} + \frac{d\boldsymbol{\Omega}}{dt} \times \mathbf{r}_p + \boldsymbol{\Omega} \times \frac{d\mathbf{r}_p}{dt} \right) \right] \end{aligned} \quad (6.1)$$

where the summation ranges m and s are used to distinguish the two agglomerate branches that are linked by the bond b . If we now use (let \mathbf{I} be the moment of inertia tensor of the agglomerate in the stationary reference frame):

$$\mathbf{I} \frac{d\boldsymbol{\Omega}}{dt} = \sum_{m\&s} [\mathbf{r}_p \times \mathbf{F}_p] - \frac{d\mathbf{I}}{dt} \boldsymbol{\Omega} \quad \text{and} \quad \frac{d\mathbf{U}_{cm}}{dt} = \sum_{m\&s} \left[\frac{\mathbf{F}_p}{m_a} \right]$$

equation (6.1) can be re-arranged as:

$$\mathbf{F}_b = \sum_m \left[\mathbf{F}_p - m_p \left(\sum_{m\&s} \left[\frac{\mathbf{F}_p}{m_a} \right] + \mathbf{I}^{-1} \left(\sum_{m\&s} [\mathbf{r}_p \times \mathbf{F}_p] \times \mathbf{r}_p \right) + \mathbf{C}_m \right) \right] \quad (6.2)$$

where \mathbf{C}_m represents all terms that do not depend on the hydrodynamic force \mathbf{F}_p , but instead are associated with the centripetal acceleration of the solid body motion of the agglomerate.

The cross-products of \mathbf{F}_p and \mathbf{r}_p cross-correlate the individual component of \mathbf{F}_b with all components of \mathbf{F}_p . If we assume, however, that characteristic values of the magnitude of the individual components of \mathbf{F}_p are well represented by the characteristic values of the magnitude of \mathbf{F}_p itself, equation (6.2) can be simplified to the form:

$$|\mathbf{F}_b| \propto N_m \left[|\mathbf{U}_f - \mathbf{U}_p|_m - \frac{N_m}{N_m + N_s} |\mathbf{U}_f - \mathbf{U}_p|_{m\&s} \right] + \mathbf{C}_m \quad (6.3)$$

where N_m represents the number of particles in agglomerate branch m and N_s the number of particles in branch s .

The constant term \mathbf{C}_m (and, likewise, \mathbf{C}_s), typically has a small ($<10\%$)† contribution to the magnitude of the total induced stress $|\mathbf{F}_b|$. Therefore, we can assume that the induced stresses inside the agglomerate effectively only depend on the slip velocity of the primary particles for deriving a simplified model for the agglomerate mass. In order to proceed, we further simplify equation (6.3). We assume that the characteristic values of $|\mathbf{U}_f - \mathbf{U}_p|$ in branch m , in branch s , as well as over the entire agglomerate, change by a similar factor if the number of primary particles in the agglomerate changes. Furthermore, we assume that the relative fragmentation of the agglomerates (that is, the ratio of the number of primary particles that end up in the branches m and s) is independent of the value of F_L^* . In that case, the total number of primary particles N_{bu} in an agglomerate that is broken at a given value of F_L^* is proportional to:

$$N_{bu} \propto \frac{F_L^*}{|\mathbf{U}_f - \mathbf{U}_p|_{m\&s}} \quad (6.4)$$

† This is substantially smaller than the results found by Derksen (2008), who found that the contribution of the centrifugal force to the *average* force induced in the bond in a sphere doublet is between 35% and 50%. This discrepancy can be explained by the fact that we consider conditions *at break-up* (typically at a high of the turbulence contribution) and wall-bounded flows instead of homogeneous turbulence, thereby also including the effect of a mean velocity gradient.

Similarly, the value of N_{bu} for agglomerates that are broken by bending or twisting is expected to scale as:

$$N_{bu} \propto \left[\frac{T_L^*}{|\mathbf{U}_f - \mathbf{U}_p|_{m\&s}} \right]^{D_f/(1+D_f)} \quad (6.5)$$

where D_f is the fractal dimension of the agglomerates.

6.3. Scaling of mean mass of agglomerates at break-up

Given the dependence of the slip velocity shown in figure 5, it is to be expected that for one-way coupling, the mean mass of the agglomerates at break-up scales with F_L^* to a power smaller than one. For two-way coupling, larger scaling exponents, which vary with the value of Re_∇ are expected, because $|\mathbf{U}_f - \mathbf{U}_p|$ is found to vary with the Reynolds number in this case. Finally, because the slip velocities are larger in the pipe than in the channel, the agglomerate mass is expected smaller in the pipe compared to the channel at the same agglomerate strength.

Figure 6 shows the dependence of the mean mass of the agglomerates at the moment that the agglomerates are broken (\bar{N}_{bu}) as observed in our simulations. The solid lines in figure 6 are least-square fits that relate the mean mass of the agglomerates to the value of F_L^* or T_L^* for one-way coupling. As expected, the scaling exponents for two-way coupling are larger than for one-way coupling; also the two-way coupled scaling exponents indeed show some dependence on the Reynolds number. For one-way coupling, the scaling exponents are slightly larger than expected based on expressions (6.4) and (6.5). This discrepancy can be explained by considering that the simplified model does not account for possible variations in the direction of the hydrodynamic force exerted on different primary particles in each of the branches of the broken agglomerate. This variation, which will reduce the ability of the force to constructively contribute to the stress that is induced in the bond, will decrease as the agglomerates become larger. It thus will give rise to a higher scaling exponent between \bar{N}_{bu} and F_L^* or T_L^* compared to the predictions given in expressions (6.4) and (6.5).

An interesting observation in figure 6 is that even though the mean mass of the agglomerates in general indeed is smaller in the pipe than in the channel, the values of \bar{N}_{bu} increase much more strongly at large values of F_L^* and T_L^* in the pipe. We propose that the wall-normal concentration profile, in conjunction with the fact that the cross-sectional area of centre of the pipe is a lot smaller when compared to the area centred around the midplane of the channel, explains the differences in \bar{N}_{bu} . As an example, let us consider an agglomerate that is located at a dimensionless wall-normal coordinate of 0.45 in both geometries (viz. at $z = 0.45$ or $z = 0.55$ in the channel, or at $r = 0.05$ in the pipe). Upon break-up, the agglomerate branches that are moving apart in the transversal direction have the full channel width ($2H$) at their disposal, before possibly touching again at the other side due to the periodic boundary conditions. The equivalent distance in the pipe geometry is 0.05π times the pipe diameter, which is just 8% of the distance available in the channel. Only from a wall-normal coordinate of 0.18 outwards, the circumference of the pipe becomes larger than the width of the channel. Agglomerates that are present close the centre of the pipe thus have a larger chance of re-colliding shortly after they are being broken, thereby growing to larger dimensions than in the channel.

6.4. Fractal dimension

The agglomerates formed in our simulations have a very open, porous structure. Even though the agglomerates arguably contain too few primary particles $\mathcal{O}(100 - 1000)$ to

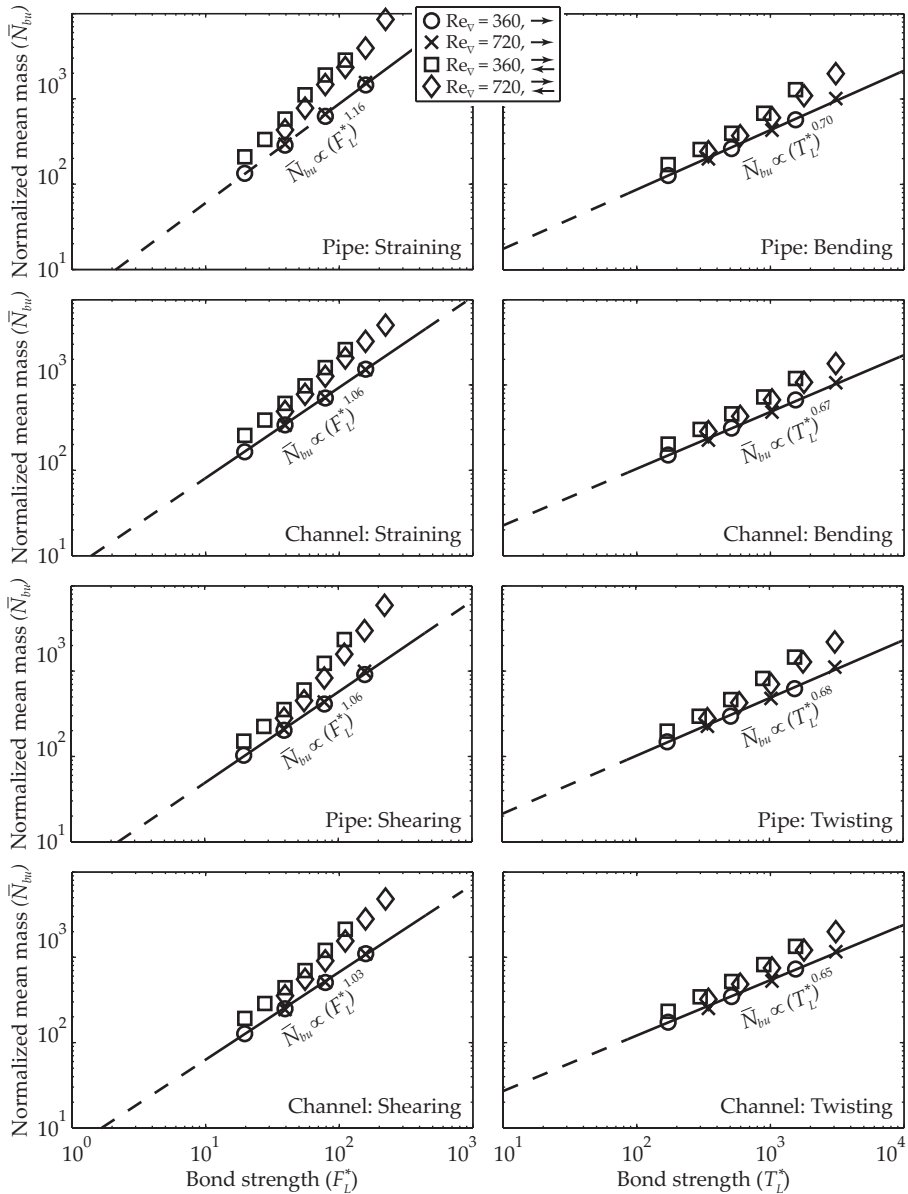


FIGURE 6. Scaling of the mean agglomerate mass *at agglomerate break-up* (\bar{N}_{bu}).

qualify as proper fractal objects, attributing a fractal dimension to them is instructive to assess their structure. The mass-fractal dimension D_f is defined as:

$$m_a \propto R_g^{D_f} \quad (6.6)$$

where m_a represents the mass of an individual agglomerate and R_g is a representative radius of the agglomerates. In this work, we use the radius of gyration for representing

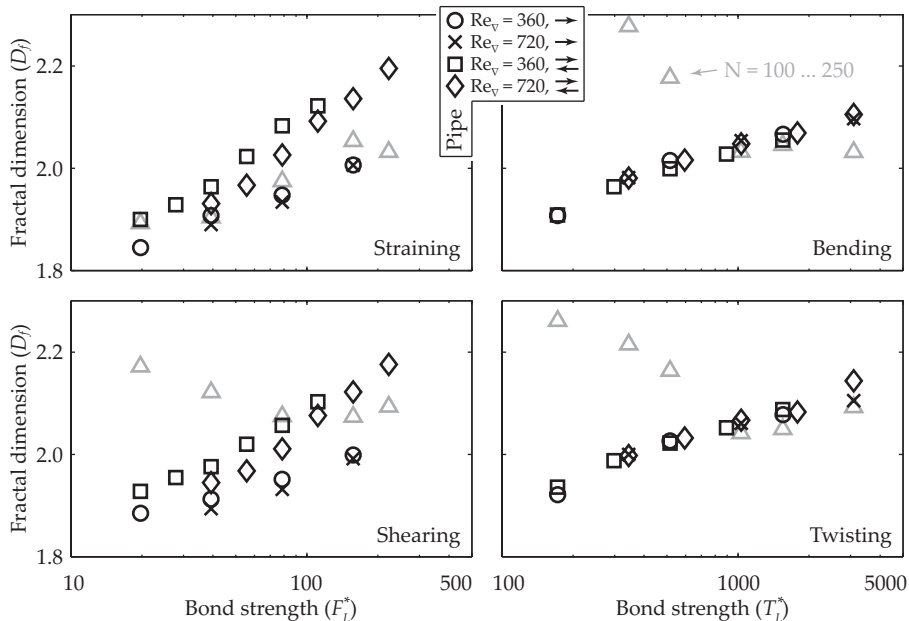


FIGURE 7. Overall fractal dimensions for steady-state agglomerate populations for the different cases considered, amended by average fractal dimensions for a subset of agglomerates (with $N = 100 - 250$). The supplementary material shows the same figure, though with inclusion of the channel results.

the agglomerate radius, which is defined as:

$$R_g \equiv \sqrt{\frac{1}{N} \sum_p (\mathbf{r}_p \cdot \mathbf{r}_p)} \quad (6.7)$$

where the sum runs over all N primary particles in the agglomerate.

To determine the fractal dimension of the agglomerates, a large ensemble of (m , R_g) data points is obtained from steady-state agglomerate populations. This ensemble is subsequently divided into 100 sections of increasing agglomerate mass, and for each of these sections, the average value of R_g is determined; subsequently expression (6.6) is fit to these data to obtain the fractal dimension of the agglomerates. Figure 7 summarises the results obtained this way.

For the overall fractal dimension (putting – for the moment – aside the datapoints marked with $N = 100 - 250$), a general monotonic increase of D_f is found with increasing values of F_L^* and T_L^* . Break-up and subsequent re-agglomeration is known to increase the fractal dimension of agglomerates (Lazzari *et al.* 2016). The overall fractal dimensions span the range reported by Meakin & Jullien (1988) for the mechanism that is closest to our model (diffusion limited aggregation) without and with restructuring ($D_f = 1.80$ and $D_f = 2.18$, respectively). Confirming visual observations, the range of fractal dimensions obtained indicates that the agglomerates have a very open, porous, structure.

Since the fractal dimension is a measure of the degree of compactness of the agglomerates, differences in the fractal dimension are related to the degree of inter-penetration that agglomerates attain before colliding. As the number of primary particles per agglomerate is still relatively small in our simulations, the voids in the agglomerates will become larger with respect to the primary particle size when the agglomerates become larger.

Therefore, inter-penetration becomes more easy as agglomerates grow and this way, the general increase of D_f with F_L^* and T_L^* can be understood. Agglomerate branches that consist of only a small number of primary particles can easily protrude into the matrix of another, larger agglomerate branch. It therefore may be expected that agglomerate re-structuring, caused by subsequent break-up and collision events within the same agglomerate, is dominated by those break-up events in which one of the branches of the broken agglomerate contains much less primary particles than the other branch. If such an event occurs, the question whether the agglomerate will re-structure into a more compact or a more open form depends on the relative motion of both agglomerate branches after they are being broken apart.

Accepting this re-structuring mechanism enables to explain the influence of two-way coupling and of the Reynolds number on the fractal dimension of the agglomerates. Since the inertia of the agglomerates is relatively low, small agglomerate branches can quickly adapt to the local fluid velocity fluctuations that occur in the turbulent flow. Therefore, the chance that a small agglomerate branch can escape from the vicinity of its large counterpart increases when the intensity of the turbulence increases. Agglomerates will thus become less compact (and have a smaller fractal dimension) when the Reynolds number is increased, and more compact when the turbulence fluctuations (and thus the local fluid velocity differences surrounding both agglomerate branches) are damped due to two-way coupling. Since the impact of two-way coupling compared to one-way coupling is stronger in the pipe than it is in the channel, this effect also explains the stronger increase of the fractal dimension with the strength of the inter-particle bonds found in the two-way coupled pipe flow simulations when compared to the channel flow (as shown in the supplementary material). As the effective turbulence intensity as felt by the dispersed phase is larger in the pipe than in the channel due to the relative expansion of the turbulent inner layer, this effect also contributes to the general decrease of D_f in the pipe compared to the channel.

To better understand how the fractal dimension of the agglomerates varies within an agglomerate population, results on the fractal dimension of a subset of agglomerates (with $N = 100$ to 250) that are present in all simulations are also shown in Figure 7. These fractal dimension are averaged over all flow conditions considered and will be denoted by $D_f^{100-250}$. It is important to appreciate that the $N = 100 - 250$ subset of the agglomerates comprise some of the largest of the population at small values of F_L^* or T_L^* . Contrary, at large strengths, this subset comprises the smallest agglomerates present. The larger the value of D_f is, the smaller are the dimensions of an agglomerate that consists of a given number of primary particles. Large values of D_f therefore enhance the chance that many primary particles of an agglomerate are surrounded by the same turbulent eddy. In turn, this increases the likelihood that the external force that acts on the particles is directed roughly in the same direction. As the latter may allow a small branch to harvest sufficient external force to break free from its parent agglomerate, large values of D_f promote the formation of agglomerate branches that are small compared to the total population. Contrary, having open structure is beneficial for forming relatively large agglomerates. The relative size of the $N = 100 - 250$ agglomerates in the total population depending on the agglomerate strength thus explains the relation between $D_f^{100-250}$ and F_L^* for straining.

For agglomerates that are broken by bending and twisting, the situation is different. This is because the induced torque scales with the hydrodynamic force per primary particle as well as the linear dimensions of the agglomerate (and thus with R_g). Small agglomerates at large values of T_L^* are more easily formed if they have a small D_f (and thus a large R_g), whereas large agglomerates at small values of T_L^* require a small R_g

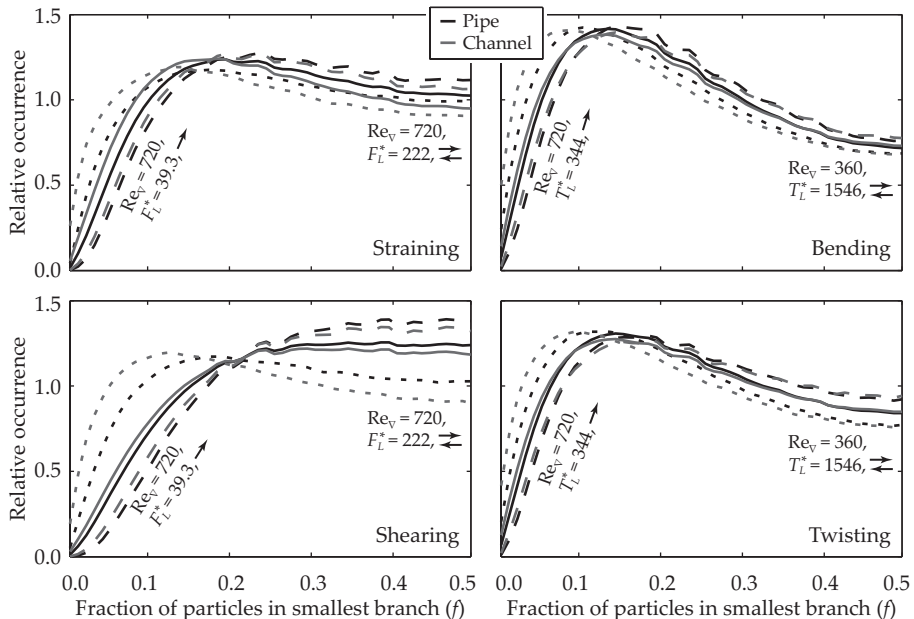


FIGURE 8. Histogram of the fraction of the primary particles that end up in the smallest agglomerate branch during a break-up event. Solid lines: averaged results over all cases considered per break-up mechanism, dashed lines: extreme cases as indicated by the labels shown.

(and a large D_f) to survive against break-up by the induced torque. This is in line with the findings shown in Figure 7. However, we have no explanation for why the relation between $D_f^{100-250}$ and F_L^* for shearing is more similar to bending and twisting than straining (despite the induced stress being independent of R_g in that case).

The disparity between D_f and $D_f^{100-250}$ for a given value of F_L^* and T_L^* shows that the agglomerate populations formed in our simulations cannot be characterised by a single fractal dimension. Instead, there is a range of fractal dimensions depending on their relative size compared to the whole agglomerate population.

7. Results: Relative fragmentation of agglomerates

A common assumption made in break-up models proposed in the literature is that agglomerates break in two branches of equal mass (binary breakage). de Bona *et al.* (2014) studied break-up of agglomerates smaller than the Kolmogorov scale in isotropic turbulent flows, and found agglomerate fragments of all sizes are produced, with an approximately linear relation between the size of the fragments formed and the frequency (hardly any single primary particles on the one hand and binary breakage with the highest probability on the other hand).

Figure 8 shows a histogram of the fraction of the number of primary particles of the agglomerate that end up in the branch that contains the smallest number of the primary particles in our work. The results in figure 8 clearly show that in our simulations, binary breakage, which would be represented by a δ -function at $f = 0.5$, is a poor representation of the relative fragmentation of the agglomerates. On average, the distribution is skewed towards forming one branch that contains a minority and one branch that contains the majority of the primary particles of the agglomerate that is being broken. In accordance

to these results we find that the most-stressed bonds typically are located in the internal parts of the agglomerate. The same was reported by Gastaldi & Vanni (2011).

Increasing values of F_L^* and T_L^* are found to produce more asymmetric fragmentation of the agglomerates, as do decreasing values of the Reynolds number, as well as two-way coupling instead of one-way coupling. We propose that these effects can be explained by the fact that any of the aforementioned parameters increases the \bar{N}_{bu} of the agglomerates. In agglomerates that consist of a large number of primary particles, the number of bonds between primary particles that experience an induced stress that exceeds the strength of the bonds will be larger than in agglomerates that are made up of a smaller number of primary particles. Since, in our break-up model, the actual bond in the agglomerate that is being broken if multiple bonds in an agglomerate are eligible for break-up is selected randomly, the chance that an agglomerate is broken in asymmetric branches can be expected to increase if the number of primary particles inside the agglomerate increases. This is also part of the reason that a different result is found compared to the work of de Bona *et al.* (2014). In their model, agglomerates were broken at the location where the internal stress is highest. Therefore, the said smoothing of the fragmentation yield found in our model is not present in their work. Furthermore, de Bona *et al.* studied homogeneous isotropic turbulence instead of wall-bounded flows, thereby also reducing the change asymmetric agglomerate fragments are formed (e.g. if a relatively small branch of an agglomerate is located in the inner layer of the turbulent flow and the rest of the agglomerate is located in the outer layer).

The fact that break-up by bending and twisting produces more asymmetric break-up fragments than straining and shearing can be understood from the fact that the induced torque in the bonds scales both with the force and the agglomerate radius. A small branch that is located relatively far away from the centre of mass of an agglomerate can more easily induce a large torque in the inter-particle bond that keeps it attached to the agglomerate than it can induce a large force.

8. Conclusions

Dispersed primary particles that undergo agglomeration and break-up have a very different interaction with the turbulent flow compared to non-interacting particles. The interaction between the turbulence and the dispersed phase proceeds by two competing mechanisms that both originate from the fact that the dispersed phase acts as a spatial filter of the fluid velocity field. On the one hand, a reduction of turbulent velocity fluctuations occurs, while on the other hand, a long-range correlation in the fluid velocity field is introduced. Which of these two mechanisms is dominant depends on the size of the agglomerates formed and thereby, a maximum increase in flow rate at intermediate values of the strength of the inter-particle bonds in the dispersed phase is found.

The mass of the agglomerates formed can be predicted quite accurately from the mean value of the slip velocity of the individual primary particles. This slip velocity depends on the coupling mode used, on the flow geometry, as well as on the Reynolds number of the turbulent flow (the latter under two-way coupling only). Little variation as a function of the break-up mode is found, apart from a clear distinction between straining and shearing on the one hand (where masses scale approximately with F_L^* to the first order), and bending and twisting on the other hand (where masses scale approximately with T_L^* to order two-thirds, which is consistent with the fractal dimension of the agglomerates). The fractal dimension of the agglomerates itself is consistent with classical results from the literature, showing that a turbulent flow as the driving force for building the agglomerates does not lead to fundamentally different agglomerate properties. Depending on the

mechanism by which agglomerates are broken different relations between the fractal dimension of a fixed-size subset of the agglomerates and the bond-strength is found, however, that partly can be explained by the interaction between the agglomerates and the turbulence.

For all break-up mechanisms, the fragmentation yield, measured by the fraction of primary particles that end up in the branches that are formed during break-up events, is asymmetric. Binary breakage, is found to be a poor representation of the actual break-up process, even though it is frequently used as a break-up mechanism in engineering models. Our results show that agglomerates are most likely to break into parts that contain approximately one quarter and three quarters of the primary particles that originally were contained in the agglomerate that is broken.

9. Acknowledgements

This research was carried out within the context of the ISAPP Knowledge Centre. ISAPP (Integrated Systems Approach to Petroleum Production) is a joint project of the Netherlands Organization for Applied Scientific Research (TNO) and Delft University of Technology, sponsored by Eni, Petrobras, and Statoil.

REFERENCES

- BABLER, M. U. 2008 Collision efficiency model for flow-induced coagulation of fractal aggregates. *AIChE Journal* **54**, 1748–1760.
- BABLER, M. U., BIFERALE, L., BRANDT, LUCA, FEUDEL, ULRIKE, GUSEVA, K., LANOTTE, A. S., MARCHIOLI, C., PICANO, F., SARDINA, G., SOLDATI, A. & TOSCHI, F. 2015 Numerical simulations of aggregate breakup in bounded and unbounded turbulent flows. *J. Fluid Mech.* **766**, 104–128.
- BALACHANDAR, S. & EATON, J. K. 2010 Turbulent dispersed multiphase flow. *Annu. Rev. Fluid Mech.* **42**, 111–133.
- BOERSMA, B. J. 1997 Electromagnetic effects in cylindrical pipe flow. PhD thesis, Delft University of Technology.
- DE BONA, J., LANOTTE, A. S. & VANNI, M. 2014 Internal stresses and breakup of rigid isostatic aggregates in homogeneous and isotropic turbulence. *J. Fluid Mech.* **755**, 365–396.
- BRUNK, B. K., KOCH, D. L. & LION, L. W. 1998 Turbulent coagulation of colloidal particles. *J. Fluid Mech.* **364**, 81–113.
- CHEN, D. & DOI, M. 1999 Microstructure and viscosity of aggregating colloids under strong shearing force. *J. Colloid Interf. Sci.* **212**, 286–292.
- CHEN, M., KONTOMARIS, K. & MCLAUGHLIN, J. B. 1998 Direct numerical simulation of droplet collisions in a turbulent channel flow. part i: collision algorithm. *Int. J. Multiph. Flow* **24**, 1079–1103.
- CROWE, C. T., SOMMERFELD, M. & TSUJI, Y. 1997 *Multiphase flows with droplets and particles*. CRC Press.
- DERKSEN, J. J. 2008 Flow-induced forces in sphere doublets. *J. Fluid Mech.* **608**, 337–356.
- DERKSEN, J. J. 2012 Direct numerical simulations of aggregation of monosized spherical particles in homogeneous isotropic turbulence. *AIChE Journal* **58**, 2589–2600.
- DIZAJI, F. F. & MARSHALL, J. S. 2016 An accelerated stochastic vortex structure method for particle collision and agglomeration in homogeneous turbulence. *Phys. Fluids* **28**, 113301.
- EGGELS, J. G. M. 1994 Direct and large eddy simulation of turbulent flow in a cylindrical pipe geometry. PhD thesis, Delft University of Technology.
- ERNST, M., DIETZEL, M. & SOMMERFELD, M. 2013 A Lattice Boltzmann method for simulating transport and agglomeration of resolved particles. *Acta Mech.* **224**, 2425–2449.
- FLESCH, J. C., SPICER, P. T. & PRATSINIS, S. E. 1999 Laminar and turbulent shear-induced flocculation of fractal aggregates. *AIChE Journal* **45**, 1114–1124.

- GASTALDI, A. & VANNI, M. 2011 The distribution of stresses in rigid fractal-like aggregates in a uniform flow field. *J. Colloid Interf. Sci.* **357**, 18–30.
- VAN HAARLEM, B. A. 2000 The dynamics of particles and droplets in atmospheric turbulence: A numerical study. PhD thesis, Delft University of Technology.
- JOHNSON, K. L., KENDALL, K. & ROBERTS, A. D. 1971 Surface energy and the contact of elastic solids. *Proc. R. Soc. A* **324**, 301–313.
- KHOURY, G. K. EL, SCHLATTER, P., NOORANI, A., FISCHER, P. F., BRETHOUWER, G. & JOHANSSON, A. V. 2013 Direct numerical simulation of turbulent pipe flow at moderately high Reynolds numbers. *Flow Turbul. Combust.* **91**, 475–495.
- LAZZARI, S., NICOUD, L., JAQUET, B., LATTUADA, M. & MORBIDELLI, M. 2016 Fractal-like structures in colloid science. *Adv. Colloid Interface Sci.* **235**, 1–13.
- LI, Y., MCLAUGHLIN, J. B., KONTOMATIS, K. & PORTELA, L. 2001 Numerical simulation of particle-laden turbulent channel flow. *Phys. Fluids* **13**, 2957–2967.
- MÄKINEN, J. T. T. 2005 Particle accretion and dissipation simulator: Collisional aggregation of icy particles. *Icarus* **177**, 269–279.
- MARCHIOLI, C., SOLDATI, A., KUERTEN, J. G. M., ARZEN, B., TANIÈRE, A., GOLDENSOPH, G., SQUIRES, K. D., CARGNELUTTI, M. F. & PORTELA, L. M. 2008 Statistics of particle dispersion in direct numerical simulations of wall-bounded turbulence: Results of an international collaborative benchmark test. *Int. J. Multiph. Flow* **34**, 879–893.
- MEAKIN, P. & JULLIEN, R. 1988 The effects of restructuring on the geometry of clusters formed by diffusion-limited, ballistic, and reaction-limited cluster–cluster aggregation. *J. Chem. Phys.* **89**, 246–250.
- MOSER, R. D., KIM, J. & MANSOUR, N. N. 1999 DNS of turbulent channel flow up to $Re_\tau = 590$. *Phys. Fluids* **11**, 943–945.
- PASCHKEWITZ, J. S., DUBIEF, Y., DIMITROPOULOS, C. D., SHAFEQ, E. S. G. & MOIN, P. 2004 Numerical simulation of turbulent drag reduction using rigid fibres. *J. Fluid Mech.* **518**, 281–317.
- PORTELA, L. M., COTA, P. & OLIEMANS, R. V. A. 2002 Numerical study of the near-wall behaviour of particles in turbulent pipe flows. *Powder Technol.* **125**, 149–157.
- PORTELA, L. M. & OLIEMANS, R. V. A. 2003 Eulerian–Lagrangian DNS/LES of particle–turbulence interactions in wall-bounded flows. *Int. J. Numer. Methods Fluids* **43**, 1045–1065.
- POURQUIÉ, M. J. B. M. 1994 Large-eddy simulation of a turbulent jet. PhD thesis, Delft University of Technology.
- PTASINKSI, P. K., NIEUWSTADT, F. T. M., VAN DEN BRULE, B. H. A. A. & HULSEN, M. A. 2001 Experiments in turbulent pipe flow with polymer additives at maximum drag reduction. *Flow Turbul. Combust.* **66**, 159–182.
- READE, W. C. & COLLINS, L. R. 2000 A numerical study of the particle size distribution of an aerosol undergoing turbulent coagulation. *J. Fluid Mech.* **415**, 45–64.
- RICHARDSON, D. C. 1995 A self-consistent numerical treatment of fractal aggregate dynamics. *Icarus* **115**, 320–335.
- SCHUTTE, K. C. J. 2016 A hydrodynamic perspective on the formation of asphaltene deposits. PhD thesis, Delft University of Technology.
- SURESHKUMAR, R., BERIS, A. N. & HANDLER, R. A. 1997 Direct numerical simulation of the turbulent channel flow of a polymer solution. *Phys. Fluids* **9**, 743–755.
- ZINCHENKO, A. Z. & DAVIS, R. H. 2014 Growth of multiparticle aggregates in sedimenting suspensions. *J. Fluid Mech.* **742**, 577–617.